

POLARBEAR-2: an instrument for CMB polarization measurements

Y. Inoue^{a,b}, P. Ade^c, Y. Akiba^d, C. Aleman^{e,ab}, K. Arnold^f, C. Baccigalupi^g, B. Barch^h, D. Barron^h, A. Bender^{i,z}, D. Boettger^j, J. Borrill^{k,y}, S. Chapman^l, Y. Chinone^h, A. Cukierman^h, T. de Haan^h, M. A. Dobbs^m, A. Ducoutⁿ, R. Dunner^j, T. Elleflot^{e,ab}, J. Errard^o, G. Fabbian^g, S. Feeneyⁿ, C. Feng^p, G. Fuller^{e,ab}, A. J. Gilbert^m, N. Goeckner-Wald^h, J. Groh^h, G. Hall^h, N. Halverson^{q,aa,ac}, T. Hamada^b, M. Hasegawa^{b,d}, K. Hattori^b, M. Hazumi^{b,d,r,v}, C. Hill^h, W. L. Holzapfel^h, Y. Hori^h, L. Howe^{e,ab}, F. Irie^{r,s}, G. Jaehnig^{q,ac}, A. Jaffeⁿ, O. Jeong^h, N. Katayama^{r,s}, J. P. Kaufman^{e,ab}, K. Kazemzadeh^{a,ab}, B. G. Keating^{e,ab}, Z. Kermish^t, R. Keskitalo^{h,k}, T. Kisner^{k,y}, A. Kusaka^k, M. Le Jeune^u, A. T. Lee^{h,k}, D. Leon^{e,ab}, E. V. Linder^k, L. Lowry^{e,ab}, F. Matsuda^{e,ab}, T. Matsumura^v, N. Miller^w, K. Mizukami^{r,s}, J. Montgomery^m, M. Navaroli^{e,ab}, H. Nishino^b, H. Paar^{e,ab}, J. Peloton^u, D. Poletti^u, G. Puglisi^g, C. R. Raum^h, G. M. Rebeiz^{ab}, C. L. Reichardt^y, P. L. Richards^h, C. Ross^l, K. M. Rotermond^l, Y. Segawa^d, B. D. Sherwin^{h,ad}, I. Shirley^h, P. Siritanasak^{e,ab}, N. Stebor^{e,ab}, R. Stompor^u, A. Suzuki^{h,y}, O. Tajima^{b,d}, S. Takada^x, S. Takatori^d, G. P. Teply^{e,ab}, A. Tikhomirov^l, T. Tomaru^b, N. Whitehorn^h, A. Zahn^e, and O. Zahn^h

^aInstitute of physics, Academia Sinica, Taipei, Taiwan(R.O.C.);

^bHigh energy accelerator research organization, Tsukuba, Japan;

^cSchool of Physics and Astronomy, Cardiff University, Cardiff CF10, 3XQ, UK;

^dSOKENDAI, The Graduate Institute for Advanced Studies, Hayama, Miura District, Kanagawa 240-0115, Japan;

^eCenter for Astrophysics and Space Science, University of California, San Diego, CA, 92093, USA;

^fDepartment of Physics, University of Wisconsin, Madison, WI, 53706, USA;

^gScuola Internazionale Superiore di Studi Avanzati (SISSA), Via Bonomea 265, 34136, Trieste, Italy;

^hDepartment of Physics, University of California, Berkeley, CA, 94720, USA;

ⁱArgonne National Laboratory, Argonne, IL 60439, USA;

^jDepartment of Astronomy, Pontifica University Catolica de Chile, Santiago, Chile;

^kComputational Cosmology Center, Lawrence Berkeley National Laboratory, Berkeley, CA 94720 USA;

^lDepartment of Physics and Atmospheric Science, Dalhousie University, Halifax, NS, B3H 4R2, Canada;

^mPhysics Department, McGill University, Montreal, QC, H3A 0G4, Canada;

ⁿDepartment of Physics, Blackett Laboratory, Imperial College London, London SW7 2AZ UK;

^oSorbonne Universites, Institut Lagrange de Paris (ILP), 75014 Paris, France;

^pDepartment of Physics and Astronomy, University of California, Irvine, CA, 92697, USA;

^qCenter for Astrophysics and Space Astronomy, University of Colorado, Boulder, CO, 80309, USA;

^rKavli IPMU (WPI), UTIAS, The University of Tokyo, Kashiwa, Chiba 277-8583, Japan;

^sYokohama National University, Yokohama, Japan;

^tDepartment of Physics, Princeton University, Princeton, NJ, 08544, USA;

^uAstroParticule et Cosmologie, Univ Paris Diderot, CNRS/IN2P3,

CEA/Irfu, Obs de Paris, Sorbonne, Paris Cite, France;

^vInstitute of Space and Astronautical Studies (ISAS), Japanese Aerospace

Exploration Agency (JAXA), Sahamihara, Kanagawa 252-510, Japan;

^wObservational Cosmology Laboratory, Code 665, NASA Godard Space Flight Center, Greenbelt, MD, 20771, USA;

^xNational Institute for Fusion Science 322-6 Oroshi-cho, Toki City, GIFU Prefecture, Japan;

^ySpace Sciences Laboratory, University of California, Berkeley, CA, 94720, USA;

^zDepartment of Astronomy and Astrophysics, University of Chicago, Chicago, IL 60637, USA;

^{aa}Department of Astrophysical and Planetary Sciences, University of Colorado, Boulder, CO, 80309, USA;

^{ab}Department of Electrical and Computer Engineering, University of California, San Diego, CA, 92093, USA;

^{ac}Department of Physics, University of Colorado, Boulder, CO, 80309, USA;

^{ad}Miller Institute for Basic Research in Science, University of California, Berkeley, CA, 94720, USA;

POLARBEAR-2 (PB-2) is a cosmic microwave background (CMB) polarization experiment that will be located in the Atacama highland in Chile at an altitude of 5200 m. Its science goals are to measure the CMB polarization signals originating from both primordial gravitational waves and weak lensing. PB-2 is designed to measure the tensor to scalar ratio, r , with precision $\sigma(r) < 0.01$, and the sum of neutrino masses, Σm_ν , with $\sigma(\Sigma m_\nu) < 90$ meV. To achieve these goals, PB-2 will employ 7588 transition-edge sensor bolometers at 95 GHz and 150 GHz, which will be operated at the base temperature of 270 mK. Science observations will begin in 2017.

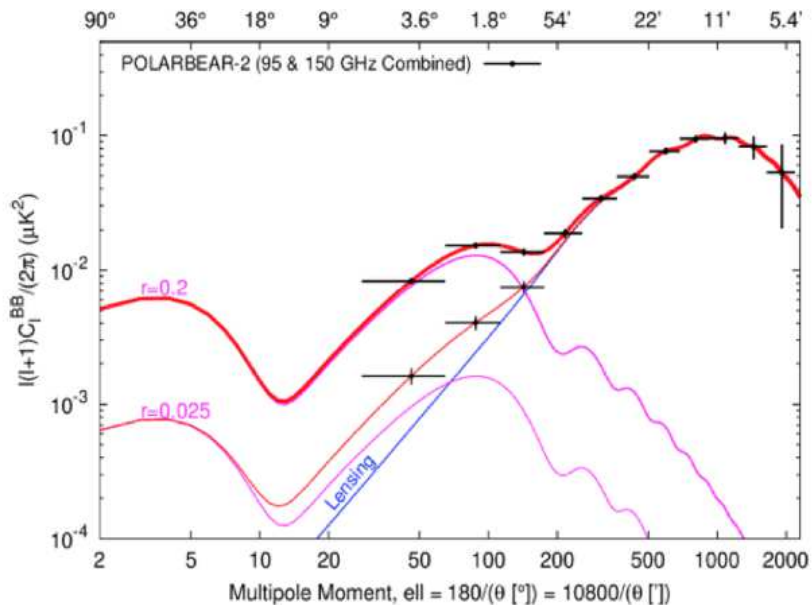


FIG. 1. Expected sensitivity of the PB-2 receiver for B-mode detection within 1 sigma errors for 3 years of observation. Pink and blue curves are the power spectra for primordial gravitational wave and gravitational lensing B-modes, respectively.

I. INTRODUCTION

PB-2 is a ground-based CMB polarization experiment with a large detector array that consists of 7588 dual-band antenna-coupled Al-Mn transition edge sensor (TES) bolometers for simultaneous measurements at 95 and 150 GHz [1, 2]. The main goal of PB-2 is to detect degree scale odd-parity (B-mode) polarization patterns [3]. The B-mode is created by primordial gravitational waves generated during the inflation [4, 5]. It is a smoking gun signature of inflationary universe. PB-2 is designed to measure the inflation models corresponding to the tensor to scalar ratio, r , with precision $\sigma(r) < 0.01$. PB-2 also plans to measure the sub-degree scale B-mode from gravitational lensing, whose amplitude is sensitive to the sum of neutrino masses, Σm_ν , with $\sigma(\Sigma m_\nu) < 90$ meV. The expected sensitivity is shown in Fig. 1. We plan to start the scientific observation from early 2017.

II. INSTRUMENT OVERVIEW

The drawing of the PB-2 receiver system is shown in Fig. 2. It consists of the box-type cryostat for the focal plane, and the optics tube for lenses and filters [6, 7]. The PB-2 receiver will be housed in a new telescope with the POLARBEAR-1 (PB-1) design [1]. The detector and refractive optical system are cooled with a combination of two pulse tube coolers and a sorption cooler [2, 8, 9]. The measured temperature and holding time of focal plane are 270 mK and 28 hours [10]. The target noise equivalent temperature (NET) of each detector is $360 \mu\text{K}\sqrt{\text{s}}$. Total array NET of each frequency is $5.8 \mu\text{K}\sqrt{\text{s}}$ and the combined array NET is $4.1 \mu\text{K}\sqrt{\text{s}}$. The specifications of PB-2 system are shown in Table. I. We mount the polarization modulator and gain calibrator into the telescope. We plan to use the sapphire half wave plate at the front of the vacuum window as the polarization modulator [11]. This modulator allows to reduce the $1/f$ noise and mitigate the beam systematics. The operation frequency is 2 Hz. The signal frequency is 8 Hz due to 4f modulation with birefringent material. We also place the chopped thermal source at the backside of secondary mirror as a gain calibrator. For the gain calibration we employ the non-polarized thermal source at 1000 K. The chopped frequencies are between 5 and 80 Hz.

III. OPTICS

The PB-2 optics consists of combination of an off-axis Gregorian telescope and alumina re-imaging lenses [6, 10]. The primary and secondary mirrors meet the Mizuguchi-Dragon condition [12, 13] to cancel the aberration and cross-

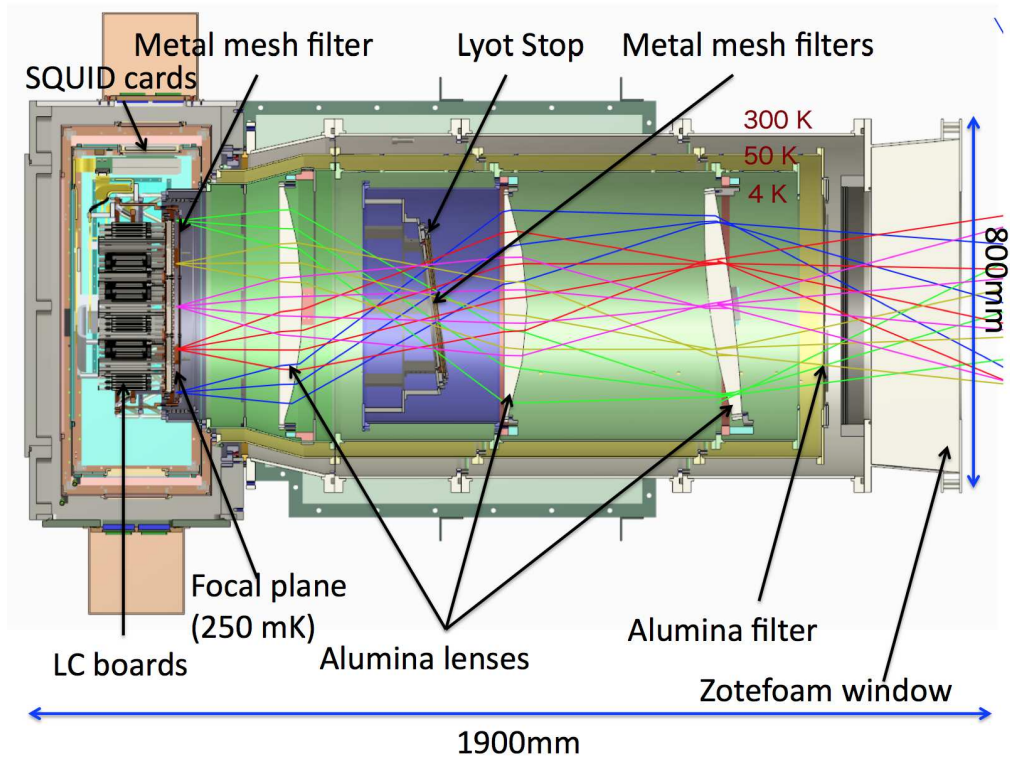


FIG. 2. Cross section of the PB-2 receiver system.

TABLE I. The summary of the PB-2 receiver specifications.

	POLARBEAR-2
Frequencies	95 GHz and 150 GHz
Number of pixels	1897 (7588 bolometers)
NET (bolometer)	$360/360 \mu\text{K}\sqrt{\text{s}}$ (95/150 GHz)
NET (array)	$5.8/5.8 \mu\text{K}\sqrt{\text{s}}$ (95/150 GHz) $4.1 \mu\text{K}\sqrt{\text{s}}$ (95 and 150 GHz combination)
Focal plane Temperature	270 mK
Field of View	4.8°
Beam Size	5.2 arcmin. @95 GHz, 3.5 arcmin. @150 GHz
Sky Coverage	80 %

polarization. The size of the primary mirror is 3.5 m in diameter projected along boresight with 2.5 m high-precision monolithic mirror and a 1 m guard ring. Its diameter corresponds to the angular resolution of 3.5 and 5.2 arcmin. at 150 and 95 GHz band, respectively. The secondary mirror is 1.5 m in diameter. The simulated beams are shown in Fig. 3. The prime focus baffle is between the primary and secondary mirror to reduce the unexpected stray light. The alumina re-imaging lenses are with 99.9 % purity from Nihon ceratech [14] and are placed at 4 K stage in the PB-2 receiver cryostat. The diameters and thicknesses of alumina lenses are 500 mm and 50 mm, respectively. The positions of the alumina lenses are measured precisely with a laser tracker. We place a Lyot stop between the aperture and collimator lenses. The Lyot stop reduced the stray light and defines the beam shapes. The edge of Lyot stop is 180 mm in diameter. We use new absorber compound named “KEK Black” as the material of the Lyot stop [10].

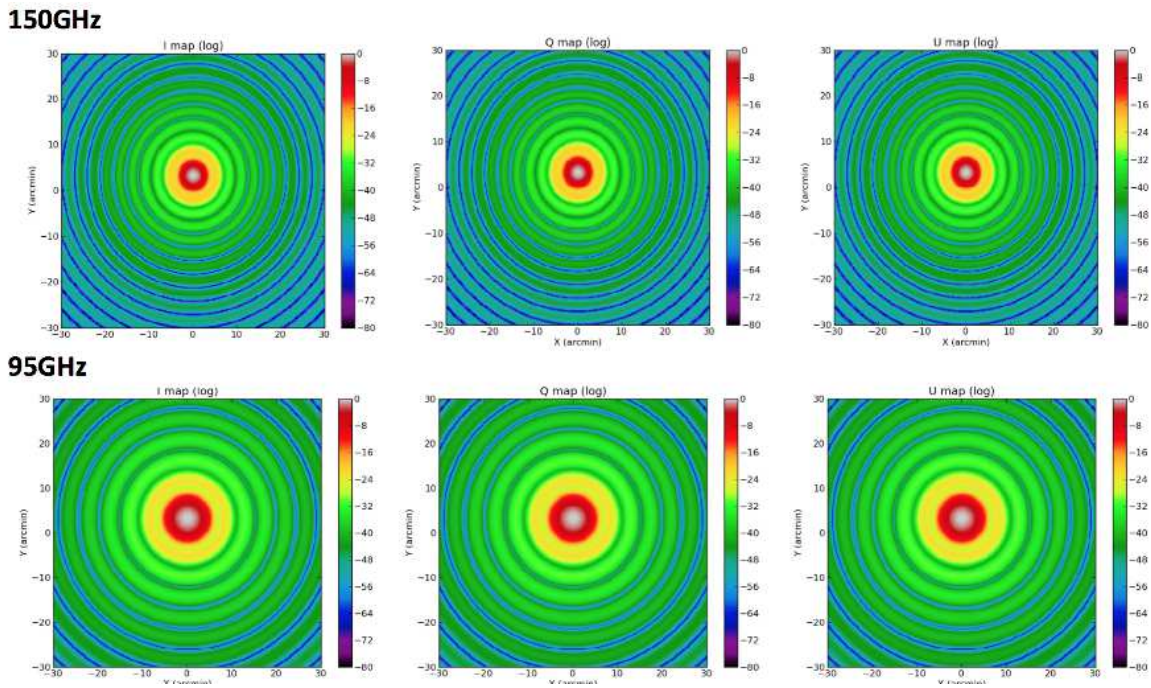


FIG. 3. Beam simulation of PB-2 optical system. I (left), Q (middle) and U (right) maps are shown for 150 GHz (top) and 95 GHz (bottom). This simulation includes the reflective alumina lenses and the Gregorian mirror system. We use the QUASt simulation [15], which is add-on software of GRASP [16].

A. Vacuum window and infrared filters

The Zotefoam [17] window is employed as the vacuum window. The refractive index of Zotefoam window is close to unity, so that we can regard it as vacuum in the range of millimeter wavelengths. The diameter and thickness of window are 800 mm and 200 mm, respectively. The measured deformation-depth of the vacuum window is 50 mm. To reduce IR emission from the window, a set of IR filters is placed at each thermal stage. The RT-MLI [18] as a 300 K filter is placed at the backside of the Zotefoam window. The cutoff frequency and temperature of RT-MLI is about 400 GHz and 168 K. We employ the alumina filter as the 50 K absorptive filter. We newly developed a high-thermal-conductivity infrared (IR) filter using alumina [7]. The diameter of alumina filter is 460 mm. We estimated the 3 dB cutoff frequency using a Fourier-transform spectrometer. The 3 dB cutoff frequency is 650 GHz [19]. The cut-off shape is steeper than that of conventional filters. The high thermal conductivity of an alumina minimizes thermal gradients. The temperature rise of the alumina filter is only 3 % of the conventional filter [6]. We also employ the metal mesh filters at 4 K and 350 mK stages. The cutoff frequencies of filters are listed in Table II.

TABLE II. IR filter specifications. All the temperatures and transmittances are measured values. The 3 dB cutoff of RT-MLI and alumina filter are quoted from elsewhere [18, 19]. The 3 dB cutoff of metal mesh filters are measured by Cardiff group.

Filter (stage)	Temperature	3 dB Cutoff	Transmittance (95 GHz)	Transmittance (150 GHz)
RT-MLI (300 K)	168 K	2000 GHz	99 %	99 %
Alumina filter (50 K)	55 K	650 GHz	96 %	96 %
Metal mesh filter (4 K)	5.8 K	360 GHz	96 %	94 %
Metal mesh filter (4 K)	5.8 K	261 GHz	98 %	94 %
Metal mesh filter (350 mK)	0.5 K	171 GHz	94 %	92 %

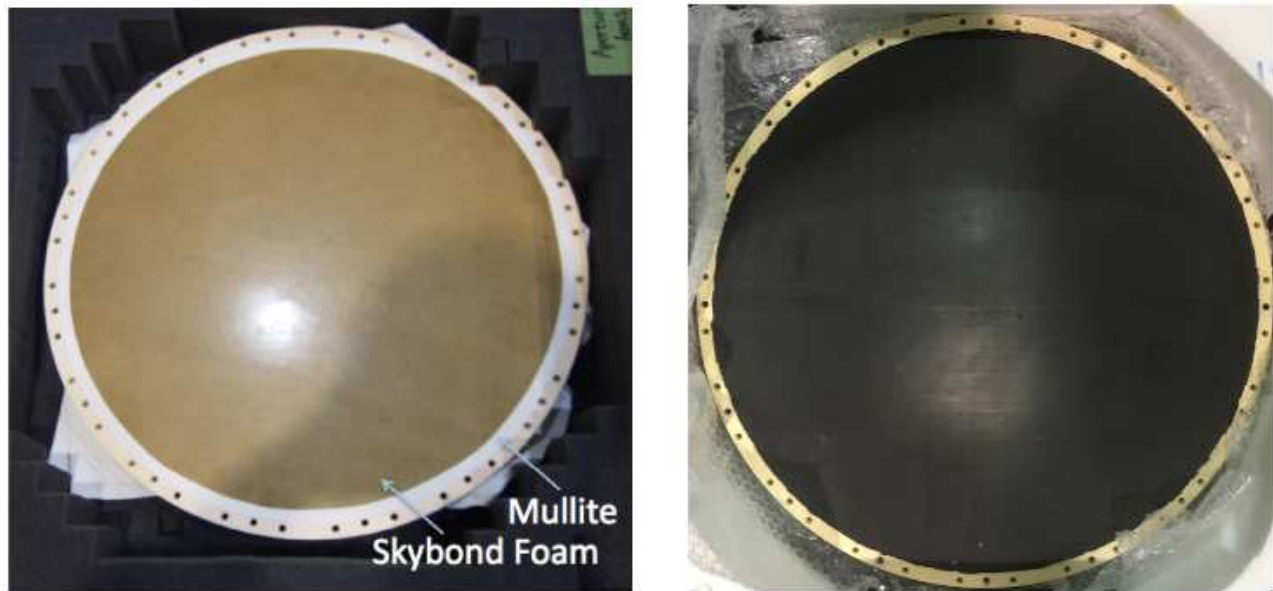


FIG. 4. Left: An alumina lens with Skybond+mullite AR coating. Right: An alumina lens with epoxy coating. We apply the Skybond+mullite AR coating on flat surfaces, and the epoxy coating on curved surfaces.

B. Anti-reflection coating

The broadband anti-reflection (AR) coating can increase the efficiency of the high-reflection optical elements, such as silicon lenslets, alumina lenses and alumina filters. The typical refractive indices of these elements are ~ 3 corresponding to 25 % reflection at the surface.

We employ the combination of two-layer AR coating methods, with Skybond + mullite [19] on the flat surfaces and with epoxy layers [7, 20] on the curved surfaces as shown in Fig. 4. The Skybond is polyimide foam made by IST corporation [21]. The thermal sprayed mullite [22, 23] is made by Tocalo corporation [24]. The epoxy coating method is with stycast 1090 and 2850FT made by Emerson & Cuming corporation [25]. Grooves are made on epoxy surfaces by laser cutting to reduce the thermal stress [7, 26].

IV. FOCAL PLANE AND DETECTOR

The focal plane with 365 mm in diameter is placed at the 250 mK stage as shown in Fig. 5. Seven hexagonal wafer modules are placed on the focal plane, which consists of detector wafers and LC boards [27, 28]. On each detector wafer, there are 271 pixels with silicon lenslets [29]. The diameter of lenslet is 6.07 mm, whose size is optimized to maximize the array NET. We place the dual-polarization sinuous antennas for broadband detection [30]. The beam map and polarization are shown in Fig. 7. The estimated beam ellipticity at 150 GHz and 95 GHz are less than 1 %. The microstrip filter separates the signal between 150 and 95 GHz, then Al-Mn TES bolometers detect the signals as shown in Fig. 6. The measured band width of the microstrip filter is shown in Fig. 7. The total number of TES bolometers is 7588.

V. READOUT

The TES bolometers are operated with electro-thermal feedback that keeps the sum of optical and electrical power to be constant [27, 28]. The resistance of TES bolometer is changed by the incident optical power, which is measured by the superconducting quantum interference devices (SQUIDS). The SQUID amplifier is operated at 4 K, coupled through a superconducting input coil. The readout channels are defined by LC filter with an inductor and a capacitor chip with each bolometer. Then, these are 60 μH inductors and capacitors made by NIST. The target of multiplexing factor is 40. The readout frequencies are between 1 and 3 MHz. The requirement of electrical cross talk is less than

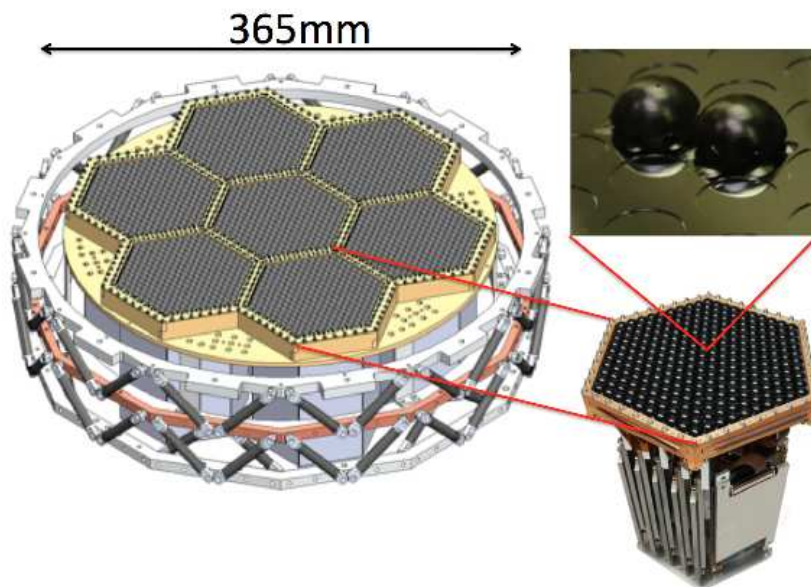


FIG. 5. Drawing of focal plane. The focal plane consists of 7 wafer modules. Each wafer module has 271 pixels. Each pixel is with a silicon lenslet.

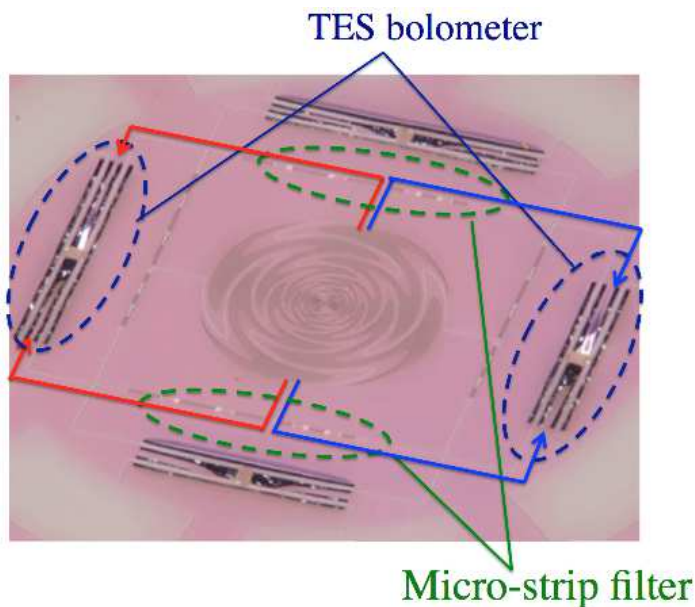


FIG. 6. Dual-band antenna-coupled Al-Mn TES bolometer. The sinuous antenna is sensitive to 95 and 150 GHz band. The microstrip filter separates the signal between 150 and 95 GHz. The separated signals are detected at TES bolometers.

1 %. The layout and spacing of LC chips are optimized with minimal cross talk. All the readout system is controlled by the ICE board [31] at room temperature as shown in Fig. 8. The overall expected readout noise is designed to be less than $7 \text{ pA}\sqrt{\text{Hz}}$.

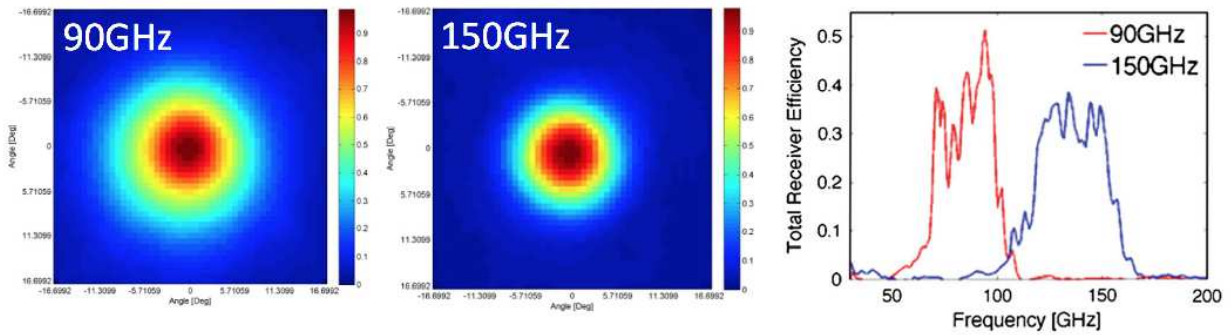


FIG. 7. Left and middle: The measured beam maps of each detector. Right: the measured bandwidth of microstrip filter.

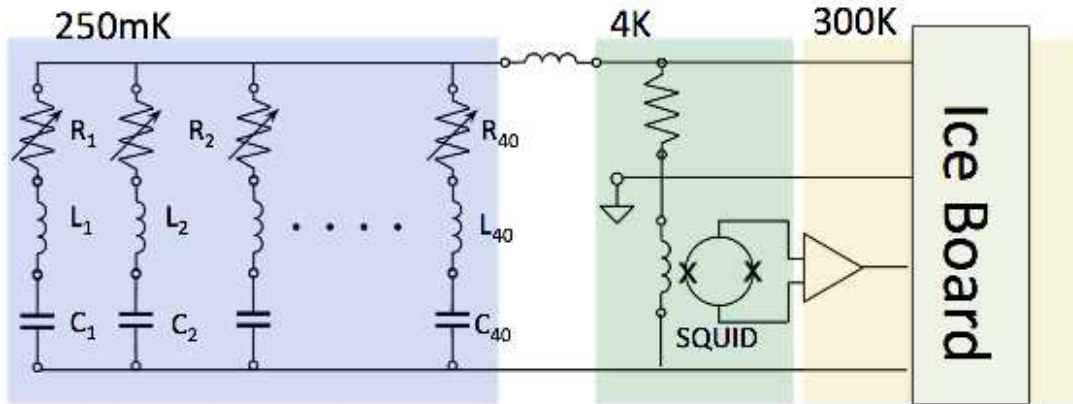


FIG. 8. The circuit of readout system. TES bolometers and LC chips are placed on 250 mK stage. We read each of the LC resonance peak with SQUID amplifier with superconducting coil. All the read out system is operated with ICE board at room temperature.

VI. SUMMARY

PB-2 is an receiver system for performing high-sensitivity observations by placing 7,588 detectors on the focal plane of 365 mm in diameter. We have developed and characterized the PB-2 receiver system for performance precision measurements of the B-mode. The PB-2 receiver system will be deployed in Chile in 2017.

ACKNOWLEDGMENTS

The POLARBRAR project is funded by the NSF under grant AST-0618398, AST-1212230 and NASA grant NNG06GJ08G. KEK authors were supported by MEXT KAKENHI Grant Numbers JP21111002, JP15H05891, and JSPS KAKENHI Grant Numbers JP13J03626, JP24740182, JP24684017, JP15H03670, JP24111715 and JP26220709. This work was supported by the JSPS Core-to-Core Program. Advanced Research Networks. The McGill authors acknowledge funding from the Natural Sciences and Engineering Research Council and Canadian Institute for Advanced Research. YI was supported by Advanced Research Course in SOKENDAI (The Graduate University for Advanced Studies), and by Academia Sinica under Grants No. CDA-105-M06 in Taiwan.

[1] N.Stebor et al., “The Simons Array CMB polarization experiment,” *Proc. SPIE* **9914**, 9914–54 (2016).
 [2] T.Tomaru et al., “The POLARBEAR-2 experiment,” *Proc. SPIE* **8452**, 84521H (2012).

- [3] M.Kamionkowski, A.Kosowsky, and A.Stebbins, “A Probe of primordial gravity waves and vorticity,” *Phys. Rev. Lett.* **78**, 2058–2061 (1997).
- [4] K.Sato, “First Order Phase Transition of a Vacuum and Expansion of the Universe,” *Mon.Not.Roy.Astron.Soc.* **195**, 467–479 (1981).
- [5] A.H.Guth, “The Inflationary Universe: A Possible Solution to the Horizon and Flatness Problems,” *Phys.Rev.* **D23**, 347–356 (1981).
- [6] Y.Inoue et al., “Thermal and optical characterization for POLARBEAR-2 optical system,” *Proc. SPIE* **9153**, 91533A (2014).
- [7] Y.Inoue et al., “Cryogenic infrared filter made of alumina for use at millimeter wavelength,” *Applied Optics.* **53**, 1727–1733 (2014).
- [8] Cryomec, “PT415.” <http://www.cryomech.com/products/cryorefrigerators/pulse-tube/pt415/>.
- [9] Chase Cryogenics, “He10 sorption cyocooler.” <http://www.chasecryogenics.com>.
- [10] Y.Inoue, “Development of POLARBEAR-2 receiver system for cosmic microwave background polarization experiment,” *Ph.D. thesis, SOKENDAI(The Graduate University for Advanced Studies)* (2016).
- [11] C.A.Hill et al., “Design and development of an ambient-temperature continuously-rotating achromatic half-wave plate for CMB polarization modulation on the POLARBEAR-2 experiment,” *Proc. SPIE* **9914**, 9142U–1 (2016).
- [12] C.Dragone, “Offset multireflector antennas with perfect pattern symmetry and polarization discrimination,” *Bell System Technical Journal.* **57**, 2663–2684 (1978).
- [13] Y. Mizugutch, M. A. and Yokoi, H., “Offset dual reflector antenna,” *IEEE Antennas and Propagation Society International Symposium* **14**, 2–5 (1976).
- [14] Nihon Ceratech. <http://www.ceratech.co.jp>.
- [15] TICRA, “QUAST.” <http://www.ticra.com/products/software/grasp/quasi-optical-design-and-analysis-add>.
- [16] TICRA, “GRASP.” <http://www.ticra.com/products/software/grasp>.
- [17] Zotefoams plc, “High Density Polyethylene Foam Property Data Sheet.” <http://www.zotefoams.com/pages/de/datasheets/hd30.htm>.
- [18] J.Choi, H.Ishitsuka, S.Mima, S.Oguri, K.Takahashi, and O.Tajima, “Radio-transparent multi-layer insulation for radiowave receivers,” *Rev.Sci.Instrum.* **84**, 114502 (2013).
- [19] Y.Inoue et al., “Cryogenic infrared filter made of alumina for use at millimeter wavelength,” *Applied Optics. in preparation*.
- [20] D.Rosen et al., “Epoxy-based broadband anti-reflection coating for millimeter-wave optics,” *Applied Optics.* **52**, 8102–8105 (2013).
- [21] IST, “<http://www.istcorp.jp/>.”
- [22] O.Jeong et al., “Broadband Plasma-Sprayed Anti-reflection Coating for Millimeter-Wave Astrophysics Experiments,” *Journal of Low Temperature Physics.* **184**, 621–626 (2015).
- [23] A.Suzuki, “Multichroic bolometric detector architecture for cosmic microwave background polarimetry experiments,” *Ph.D. thesis, University of California, Berkeley* (2013).
- [24] Tocalo, “<http://www.tocalo.co.jp>.”
- [25] Emerson and Cuming, “<http://www.emersoncuming.com>.”
- [26] Z.Ahmed et al., “BICEP3: a 95GHz refracting telescope for degree-scale CMB polarization,” *Proc. SPIE* **9153**, 91531N (2014).
- [27] D.Barron et al., “Performance of a 4 Kelvin pulse-tube cooled cryostat with dc SQUID amplifiers for bolometric detector testing,” (2013).
- [28] K.Hattori et al., “Adaptation of frequency-domain readout for Transition Edge Sensor bolometers for the POLARBEAR-2 Cosmic Microwave Background experiment,” *Nucl. Instrum. Meth.* **A732**, 299–302 (2013).
- [29] P.Siritanasak, “The broadband anti-reflection coated extended hemispherical silicon lenses for polarbear-2 experiment,” *Journal of Low Temperature Physics* **184**, 553–558 (2015).
- [30] A.Suzuki et al., “Multi-chroic dual-polarization bolometric detectors for studies of the Cosmic Microwave Background,” *Proc. SPIE* **8452**, 84523H (2012).
- [31] Amy.N.Bender et al., “Digital frequency domain multiplexing readout electronics for the next generation of millimeter telescopes,” *Proc. SPIE* **9153**, 91531A (2014).